Carrier Transport in Heterojunction Nanocrystals Under Strain

ARTICLE *in* JOURNAL OF PHYSICAL CHEMISTRY LETTERS · OCTOBER 2011

Impact Factor: 7.46 · DOI: 10.1021/jz201368e · Source: arXiv

2 AUTHORS, INCLUDING:

Mark Sweeney
University of Colorado Boulder
4 PUBLICATIONS **6** CITATIONS

THE JOURNAL OF PHYSICAL CHEMISTRY Letters

Letter

pubs.acs.org/JPCL

Carrier Transport in Heterojunction Nanocrystals Under Strain

Mark C. Sweeney and Joel D. Eaves*

Department of Chemistry and Biochemistry, University of Colorado, Boulder, Colorado 80309-0215, United States

Supporting Information

ABSTRACT: We present a theory for carrier transport in semiconducting nanoscale heterostructures that emphasizes the effects of strain at the interface between two different crystal structures. An exactly solvable model shows that the interface region, or junction, acts as a scattering potential that facilitates charge separation. As a case study, we model a type-II CdS/ZnSe heterostructure. After advancing a theory similar to that employed in model molecular conductance calculations, we calculate the electron and hole photocurrents and conductances, including nonlinear effects, through the junction at steady state.

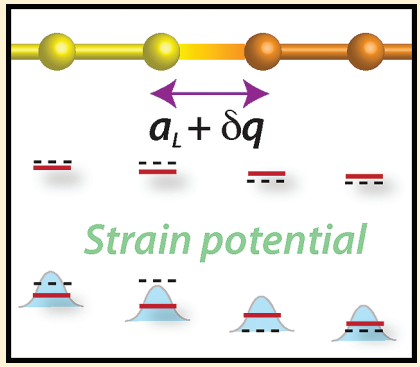

SECTION: Electron Transport, Optical and Electronic Devices, Hard Matter

Herbert Kroemer defined a semiconductor heterojunction as a "structure built from two or more different semiconductors, in such a way that the transition region or interface between the different materials plays an essential role in any device action".[1] Carriers in semiconductors, electrons and holes, experience effective forces in the vicinity of a heterostructure junction that would be impossible to generate with external fields alone. This gives one considerable freedom in manipulating the dynamics of carriers in semiconductors.[2] Because nanostructures can support larger strain fields than bulk materials, some have suggested using strain as a design element in nanoscale heterostructures.[3−6] In this Letter, we consider a semiconducting quantum rod built from two materials with different lattice constants. We presume that the strain field and the energy level offsets between the materials play the dominant role in separating electrons and holes across the junction and propose an exactly solvable model for the electron and hole transport in the device. The theory bears remarkable resemblance to the theory of conduction in molecular electronics,[7,8] where the junction between the materials is the analog of the molecule joined between two electrodes.

Nanostructures have optical and electronic properties that are tunable in ways that are simply unavailable in bulk materials. Recent advances in synthesis and characterization of semiconducting nanocrystals enable one to design structures that are optimally tailored to specific applications.[9−11] In particular, heterojunction nanocrystals can be used to harvest solar energy in a photovoltaic device or they can couple to catalysts that oxidize water to hydrogen fuel. Both of these applications require a fundamental understanding of carrier dynamics that lags behind current knowledge of electronic structure in nanocrystals.

In this Letter, we develop a theoretical description of carrier dynamics in nanocrystal heterojunctions in the presence of large strain fields. We consider a quantum rod and imagine coarse graining over a few unit cells of the rod[12] so that the system can be modeled as a 1-D chain (Figure 1). The rod is composed of two semiconductors that covalently bond at the interface, and the difference in lattice constants applies a strain field in the vicinity of the junction that joins both halves. The Hamiltonian can then be written as a sum over spatially distinct regions,

$$\mathcal{H} = \mathcal{H}_{\mathrm{L}} + \mathcal{H}_{\mathrm{R}} + \mathcal{H}_{\mathrm{J}} + \mathcal{V} \tag{1}$$

where $\mathcal{H}_{\mathrm{L}}$, $\mathcal{H}_{\mathrm{R}}$, and $\mathcal{H}_{\mathrm{J}}$ are the Hamiltonians for the left, right, and junction regions, respectively. The strain field tends to zero at the boundaries of $\mathcal{H}_{\mathrm{J}}$. $\mathcal{V}$ is the operator that couples the junction to left and right segments. In semiconductors with large dielectric constants, electron−electron interactions are weak, so we ignore them. We also ignore electron−phonon interactions, surface ligand effects,[13] spin−orbit coupling, and confinement-induced interactions. The nuclear strain field is then akin to a piezoelectric interaction and can be modeled by considering the "one-electron" part of the Hamiltonian.

To quantize the Hamiltonian, we assume that each site in the chain has two orbitals, one bonding and one antibonding. Consistent with the two band nearest-neighbor tight-binding approximation, these orbitals do not overlap, nor do the orbitals for sites that are not nearest neighbors in the chain.

Received: October 11, 2011
Accepted: December 19, 2011
Published: December 19, 2011

We assume that the number of sites in the left and right regions is large but finite. The Hamiltonian is translationally invariant away from the junction, so the transformations[14−16] that diagonalize $\mathcal{H}_L$ and $\mathcal{H}_R$ turn site orbitals into energy bands. The tight-binding approximation ignores electron−hole interactions so that the Hamiltonian separates into two sectors, the conduction (antibonding) and valence (bonding) sectors, with no coupling between them.

In addition to partitioning the Hamiltonian $\mathcal{H}$ into spatially distinct regions as in eq 1, it is convenient to partition the Hamiltonian by sector index. In our notation, the script font indicates a Hamiltonian that includes both bonding and antibonding orbitals. For example, $\mathcal{H}_L$ is the Hamiltonian for the left region of the rod, including both conduction and valence sectors. Italic fonts indicate that a Hamiltonian has been partitioned into conduction and valence sectors. H_c, for example, includes the Hamiltonian for the left and right regions, as well as the junction and the coupling between the junction and the left and right regions; but only for the conduction sector. For compactness of notation, we do not include the labels corresponding to conduction (c) and valence (v) sectors for italicized Hamiltonians partitioned into spatial regions but do discuss the analysis for H_c in detail. The analysis for H_v is identical. In the region of the junction, the strain field displaces the nuclei, and this breaks translational symmetry of the total Hamiltonian. In second quantization, H_c is

$$
\begin{aligned}
H_c &= H_L + H_R + H_J + V \\
H_L &= \sum_{k=1}^{N} \varepsilon_L(k)\hat{C}_k^{\dagger}\hat{C}_k, \\
H_R &= \sum_{q=1}^{N} \varepsilon_R(q)\hat{C}_q^{\dagger}\hat{C}_q, \\
H_J &= \sum_{n=1}^{N_J} \varepsilon_n C_n^{\dagger} C_n + \sum_{n=1}^{N_J-1} t_{n,n+1}(C_n^{\dagger} C_{n+1} \\
&\quad + C_{n+1}^{\dagger} C_n), \\
V &= C_1^{\dagger} \sum_{k=1}^{N} V_{1,k}\hat{C}_k + C_{N_J}^{\dagger} \sum_{q=1}^{N} V_{N_J,q}\hat{C}_q + \text{H. C.}
\end{aligned}
\tag{2}
$$

and similarly for H_v. H.C. denotes the Hermitian conjugate. N is the number of sites on the right and left sides, here taken to be equal, and on the same order of magnitude as the number of monolayers parallel to the interface plane in typical quantum rods. In this Letter, N is finite, and unless otherwise stated, $N = 1000$. $\hat{C}_k^{\dagger}$ is the fermionic creation operator that places an electron in Wannier orbital k on the left side, and $\hat{C}_q^{\dagger}$ creates an electron in Wannier orbital q on the right side. $\varepsilon_L(k)$ is the energy dispersion relationship for the left side and $\varepsilon_R(q)$ is the dispersion relationship for the right side (Figure 2B). ε_n and $t_{n,n+1}$ are the site energies and hopping matrix elements of the junction sites, respectively. $C_n^{\dagger}$ creates an electron at junction site n. N_J is the number of sites in the junction. Recent studies[13,17] suggest that the strain field in some nanoscale heterostructures is a few monolayers thick, so we restrict N_J accordingly. N_J varies between 1 and 5 in this study. The effects of the strain field are encoded in the tight-binding parameters, which are spatially local. To simulate a strain field, the junction site tight-binding parameters were fit to a linear interpolation between the left-side and right-side energies and hopping terms. Adjusting the tight-binding parameters in the vicinity of the junction using other interpolation schemes does not qualitatively affect the results presented here. In the tight-binding approximation, only junction site 1 couples to the left side of the rod, and junction site N_J couples to the right side with matrix elements $V_{1,k}$ and $V_{N_J,q}$, respectively.

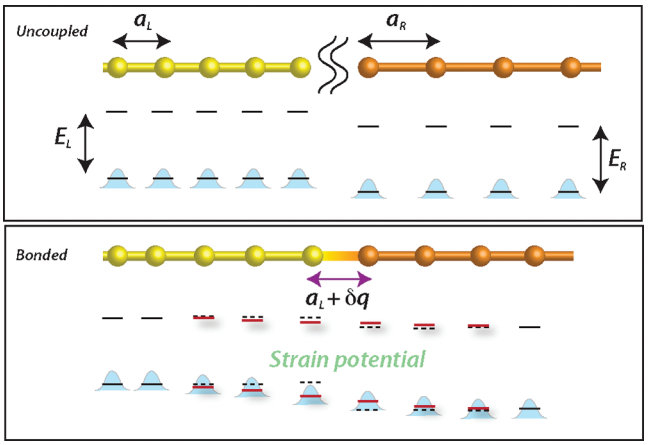

Figure 1. Schematic of the considerations that lead to the model Hamiltonian. Two semiconductors that have different lattice constants (top panel) form bonds at the interface. Each site has two orbitals, one bonding and one antibonding. The bonding−antibonding energy gap is E_L for the left side and E_R for the right. The wave functions at each site (blue curves) are sufficiently localized that one need only consider nearest-neighbor interactions. The difference in lattice constants applies a strain in the vicinity of the interface so that the equilibrium positions shift by an amount δq that is a function of the distance away from the interface. The strain field displaces the energies of the junction sites, shifting the uncoupled levels (dotted black lines) to new levels (red lines). In this cartoon, the junction consists of six sites.

The Hamiltonian in eq 2 is in the form of a quantum impurity model. Equation 2 can be understood as a multilevel Anderson−Fano model,[18,19] where each impurity level resides in the junction. As part of the analysis, we solve the impurity Green function with a hybridization function specified by the coupling between the junction and the right and left regions of the rod. Were we to include electron−electron interactions even at the level of a Hubbard term on the impurity levels, eq 2 would more closely resemble the Anderson model, which does not have an exact solution. Further details of our model Hamiltonian appear in the Supporting Information.

In photovoltaic or photocatalytic applications, photons generate electrons and holes by photoabsorption. The efficiency of electron and hole separation dictates device performance. In the case we consider, the junction facilitates electron transfer from left to right and hole transfer from right to left. The energy levels in this study are staggered and form a type-II heterojunction (Figure 2B). At the right and left regions, electrons and holes leave the rod either through a catalytic chemical reaction or through conduction to an electrode. The rod is an open system and the number of electrons and holes is not conserved, but in the steady-state situation illustrated in Figure 2A, the loss rate for electrons and holes balances the production rate from photoabsorption. The externally driven gain and loss processes occur far from the junction in our model. The steady state can be modeled by introducing quasi-Fermi levels for electrons and holes in thermodynamic averages. The difference between the quasi-Fermi

dx.doi.org/10.1021/jz201368e | J. Phys. Chem. Lett. 2012, 3, 791−795

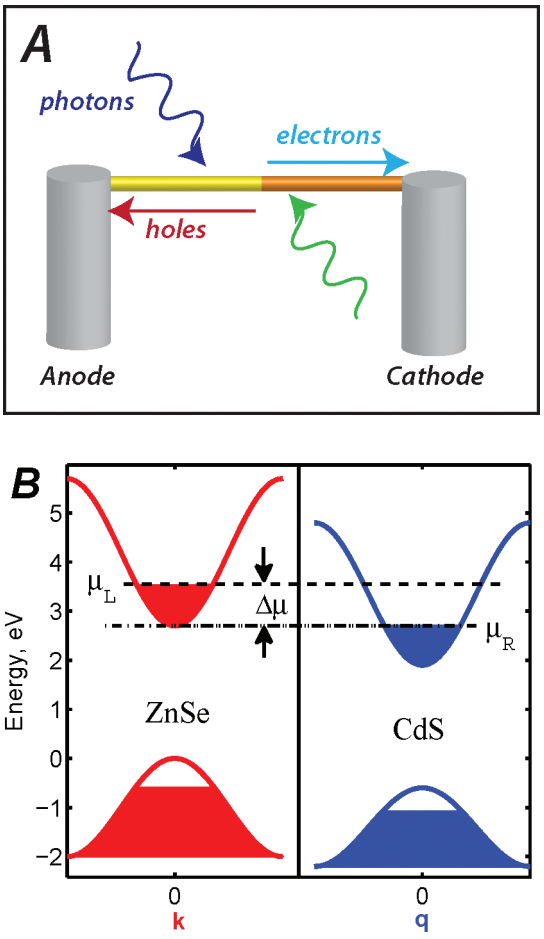

Figure 2. (A) Schematic of a nanorod heterojunction under solar illumination. This illustrates the steady state process: photons create electron–hole pairs that interact with the junction. In the steady state, the electron–hole creation and extraction processes occur far from the junction with rates that determine the mean concentrations of electrons and holes. We model the steady state by introducing quasi-Fermi levels for electrons and holes at the left and right halves of the rod. (B) Staggered ZnSe/CdS junction with bulk energy gaps of 2.7 and 2.5 eV for ZnSe and CdS, respectively. The difference in ionization energies produces a staggered junction with an energy gap of 1.9 eV between the ZnSe valence maximum and the CdS conduction minimum. The driving force is $\Delta\mu$ for the conduction bands.

levels for right and left sides is a driving force, $\Delta\mu = \mu_L - \mu_R$, and the task is to understand the rate of electron and hole transport through the junction as a function of the driving force for various junction scenarios.

One could calculate a tunneling current in terms of Green functions for left and right halves, G_L and G_R, with $H_J + V$ as a perturbation, but G_L and G_R have self-energy contributions from the junction, and the junction, in turn, has self-energies from the two sides. This is not an intractable method, but it obscures some of the physics involved.

In the tight-binding approximation, *only* the left-most and right-most sites in the junction couple to the left and right halves. In this case, the scattering formalism of Doyen[20] and Mujica[21] is exact.[22,23] The transition rate for an electron in a left-side k state to go to a right-side q state is

$$\Gamma_{qk} = \frac{2\pi}{\hbar}|T_{qk}|^2\delta(\varepsilon_L(k) - \varepsilon_R(q)) \tag{3}$$

and $T(E)$ is the transition operator

$$T(E) = V + VG(E)V \tag{4}$$

The transition operator has matrix elements, $T_{qk} \equiv \langle q|T(\varepsilon_R[q])|k\rangle$. In eq 4, $G(E)$ is the retarded Green function for the full Hamiltonian, $G(E) = [(E + i\delta)\mathbf{I} - H_0 - V]^{-1}$, where $H_0 = H_L + H_R + H_J$. Equation 4 represents a summation over multiple scattering events, which one usually solves by replacing $G(E)$ by the Dyson equation, $G(E) = G_0(E) + G_0(E)VG(E)$, and iterating to write T as a perturbation series in $G_0(E)$. In our model, however, we calculate $G(E)$ exactly. Specific steps are in the Supporting Information.

First, we write the Green function in terms of the resolvent equation, $(z\mathbf{1} - H_c)G(z) = \mathbf{1}$ for the general complex number z, then solve for the junction Green function, $G_J(z)$, from the partitioned resolvent equation. Because the left and right sides are not directly coupled, the first term in eq 4 does not contribute. The electron transfer rate for the conduction band is determined by T_{qk}, the occupancy of initial states, $f(\varepsilon_k)$, and availability, $1 - f(\varepsilon_q)$, of final states. $f(\varepsilon_k)$ is a Fermi–Dirac distribution function of the energy arguments $\varepsilon_k \equiv \varepsilon_L(k) - \mu_L$, and $\varepsilon_q \equiv \varepsilon_R(q) - \mu_R$. The current for electrons in the conduction band, j_n, is the electron transfer rate times the electron charge, e, weighted by the occupancies at steady state: $j_n = e\sum_{k,q} f(\varepsilon_k)(1 - f(\varepsilon_q))\Gamma_{qk}$. The energies near the quasi-Fermi levels make a small contribution to j_n for all but the smallest $\Delta\mu$; therefore, the Fermi–Dirac functions are approximated by step functions. After applying the step-function (zero-temperature) approximations to the Fermi–Dirac functions, the electron current is

$$j_n = \frac{2\pi e}{\hbar}\sum_{k\le k_F}\sum_{q\ge q_F}|T_{qk}|^2\delta(\varepsilon_L(k) - \varepsilon_R(q)) \tag{5}$$

Initial states need to come from $k < k_F$ and final states $q \ge q_F$, where k_F and q_F are the quasi-Fermi momenta. The nanorod is assumed to be used in a device as illustrated in Figure 2A, where electrons are transported off of the right side and holes transported off of the left side.

To determine currents, we assume that the device is operating in a regime that is limited by the transport through the junction, which implies that μ_R is fixed at or below the bottom of the left side conduction band. We vary μ_L and calculate the sums in eq 5 for each μ_L. In applications of this formalism to molecular electronics, the difference in chemical potential between right and left "leads" is equivalent to an applied voltage. Similarly, the voltage in this problem (divided by the electron charge) is the difference in quasi-Fermi levels for electrons, $\Delta\mu$. With these conventions, the differential electron conductance is the derivative of the current with respect to $\Delta\mu/e$

$$g_n = e\frac{\partial j_n}{\partial(\Delta\mu)} \tag{6}$$

The steps to derive the hole current, j_p, and conductance, g_p, are almost identical, but there need to be unoccupied hole states on the left side and occupied hole states on the right side. Hole current goes from right to left. For these calculations, the left-side quasi-Fermi level for holes, $\tilde{\mu}_L$, is fixed and the hole current and conductance is a function of $\tilde{\mu}_R$.

Values for the tight-binding parameters in the Hamiltonian, eq 2, can be rather arbitrary, but for a case study, we use CdS/ZnSe[24] as our canonical staggered heterojunction semiconductor.

dx.doi.org/10.1021/jz201368e | J. Phys. Chem. Lett. 2012, 3, 791–795

These materials have been suggested as candidates for nanoscale type-II heterostructures for photocatalytic water splitting because of their similar lattice constants, bandgaps relative to the solar emission spectrum, and energy level offsets relative to the target redox potential.[25] We fit the tight-binding parameters for left and right regions from the bulk band structure for both materials about the Γ-point. The specific tight-binding input parameters appear in the Supporting Information. Results for other materials may be obtained by fitting experimental data to a two-band tight-binding model or by electronic structure calculations.

Figures 3B,D show the electron current, j_n, and conductance, g_n, for junctions consisting of between 1 and 5 sites. Figure 3 is a plot of the full dynamic range for electron conductance and current. The sharp increase in the conductance from zero is most dramatic near the band edges, suggesting a minimum carrier density difference that one must apply to achieve efficient transport. For the right-side electron quasi-Fermi level fixed, this means that one must supply photon energy in excess of the bandgap to overcome the low conductance window. Away from the band edges the conductance is fairly uniform, suggesting that, in this regime, the device conductance should be relatively tolerant to fluctuations in the driving force. The maximum conductance is relatively insensitive to the number of the sites in the junction. The number of sites in the junction do, however, modulate the conductance modestly (~1% peak-to-peak). If the device is operating in a regime that is limited by the electron extraction rate on the right side, μ_R is shifted by ΔE to an energy level above the bottom of the conduction band for the left side. The origin of the current in Figure 3 should be shifted by ΔE.

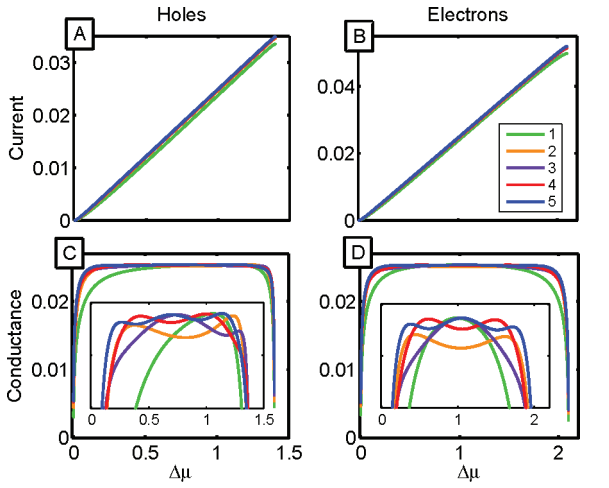

Figure 3. Current and conductance as a function of the driving force $\Delta\mu = \mu_L - \mu_R$ with junction widths of one to five sites. For the electrons (B,D) μ_R is fixed at 2.7 eV and μ_L is varied, whereas for holes (A,C) $\tilde{\mu}_L$ is fixed at −0.6 eV and $\tilde{\mu}_R$ is varied. Conductances are in units $e^2/\hbar$, currents are in units of $(e/\hbar)\bar{t}$, and the driving force is in units of $\bar{t}$. The mean hopping term $\bar{t} \equiv (t_R + t_L)/2$ is defined separately for holes and electrons. It is inversely proportional to the effective mass, and the electron-to-hole ratio for $\bar{t}$ is ~1.6. The inset plots (C,D) have a conductance range 0.025 ± 0.005 and illustrate peaks and dips in the conductance relative to the background. The peaks in the conductance are related to the resonances in the junction Green function.

The hole current and conductance are in Figures 3A and C. The hole conductances are more asymmetric than electron conductances because of the larger relative difference in the hole effective mass ($m_e^L/m_e^R = 0.97$ and $m_h^L/m_h^R = 0.8$). Because the bandwidths are inversely proportional to the effective mass, the holes have a smaller range for the driving force, and hence the maximum achievable current will be lower than that for electrons. Confinement effects do alter the effective masses of electrons and holes, but this should be straightforward to incorporate into the model.[26] We have not included them but note that they depend on the crystal orientation of the nanorod axis. In the Supporting Information, we show the details of the calculation of the T-matrix and find that $|T_{kq}|^2 \approx (m_R{}^* m_L{}^*)^{-1}$. The T-matrix elements for hole conductance should be greatly diminished in comparison with electrons, but the larger hole masses lead to larger densities of states. These two factors nearly cancel one another in the current and conductance calculations. The insets in Figures 3C and D show the fine details of the conductance values about the broad background. The stronger asymmetry in the hole conductance is due to the near coincidence of the valence band minima based on the selected tight-binding parameters. The peaks in the conductances relative to the background correspond to resonances in the junction Green function.

At the heart of the conductance calculation is the junction Green function, $G_J(E)$. In the site basis of the junction, the off-diagonal elements describe the transport properties, and the diagonal elements are related to the local density of states. In the site basis, the local density of states (LDOS) for junction site $|n\rangle$ is $-(1/\pi)\,\mathrm{Im}[\langle n|G_J(E)|n\rangle]$. To model a finite number of sites in the rod, we chose to compute self-energies in the junction Green functions using discrete sums, although the results of the semi-infinite system agree well with that computed using discrete sums for a test case of $N = 600$ (Supporting Information). The strongest peaks in G_J coincide with the band edges (Figure 4) of the left and right regions. The energy of the antibonding state for the left-most junction site is centered on the adjacent conduction band minimum or the minimum energy for the conduction band k states. (See Figure 2A.) The width of this resonance indicates that it is metastable on the time scale over which electrons flow through the junction. Because of the sharp van Hove singularity in the density of states for the left side, the lifetime of this resonance, as quantified through the imaginary part of the site self-energy, is a very sensitive function of energy (Supporting Information). Small perturbations may push this state below the conduction band minimum and lead to stabilization of the left-most junction site. The right-most junction site, on the other hand, lies within the conduction band of the right side q states. The lifetime of this state is shorter and is a weak function of energy. The situation for holes is similar but with the bonding orbital forming a metastable state on the right-hand side. We speculate that interactions not included in this model might stabilize electron and hole states on opposite sides of the junction and lead to stable trap states that intervene in the band gap. They would become populated as current flows through the rod. The bound states would correspond to an electron on one side of the junction and a hole on the other, or a dipole moment across the interface.[27−29] This dipole would further facilitate electron−hole separation across the interface, but without including electron−electron interactions, we cannot comment on this further.

This Letter presents the initial steps toward a proper theoretical description of carrier dynamics in nanocrystal heterojunctions in the presence of large strain fields. By sacrificing atomistic detail, we proposed a simplified but exactly solvable model for transport through the interface. Some of the predicted

dx.doi.org/10.1021/jz201368e | J. Phys. Chem. Lett. 2012, 3, 791−795

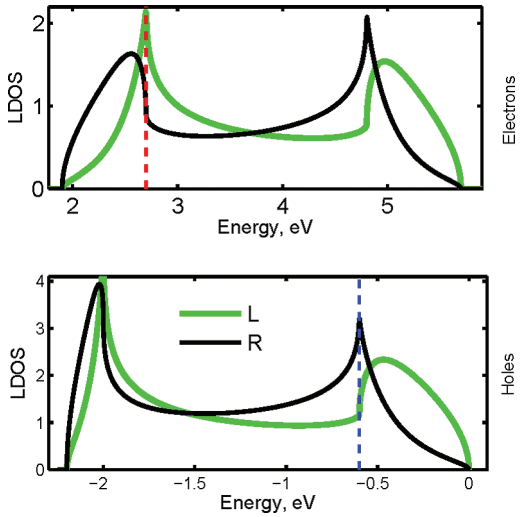

Figure 4. Local density of states (LDOS) for electrons and holes for a two site junction. R and L correspond to the right and left sites of the junction. The red dashed line indicates the nanorod left side conduction minimum at 2.7 eV. The blue dashed line is the nanorod right side valence maximum at −0.6 eV. (See Figure 2B.)

features, for example, the peaks in the conductance, might be tested by future experiments. One would obviously like to improve upon the model by including many-body interactions and study the character of the interfacial states. Specifically, excitonic effects that are ignored here can be important in strongly confined systems. The theoretical outline presented here bears strong resemblance to the theory of molecular conduction, both in form and analysis. We therefore suspect that nonequilibrium Green function methods, employed to model transport in systems with interactions,[8] might play a similar role in advancing the understanding of carrier dynamics through nanoscale heterostructures.

■ ASSOCIATED CONTENT

Supporting Information

Material contains details of the model Hamiltonian, the tight-binding parameters, transition operator derivation, and further details on the current and conductance calculations. This material is available free of charge via the Internet at http://pubs.acs.org/.

■ AUTHOR INFORMATION

Corresponding Author

*E-mail: Joel.Eaves@colorado.edu.

■ ACKNOWLEDGMENTS

J.D.E. thanks the University of Colorado for generous startup funds. We have benefited greatly from discussions with G. Dukovic.

■ REFERENCES

(1) Kroemer, H. Nobel Lecture: Quasielectric Fields and Band Offsets: Teaching Electrons New Tricks. *Rev. Mod. Phys.* **2001**, *73*, 783.
(2) Kroemer, H. Heterostructure Devices: A Device Physicist Looks at Interfaces. *Surf. Sci.* **1983**, *132*, 543−576.
(3) Yang, S.; Prendergast, D.; Neaton, J. B. Strain-Induced Band Gap Modification in Coherent Core/Shell Nanostructures. *Nano Lett.* **2010**, *10*, 3156−3162.
(4) Yang, S.; Prendergast, D.; Neaton, J. B. Nonlinear Variations in the Electronic Structure of IIVI and III-V Wurtzite Semiconductors with Biaxial Strain. *Appl. Phys. Lett.* **2011**, *98*, 152108.
(5) Antons, A.; Neaton, J. B.; Rabe, K. M.; Vanderbilt, D. Tunability of the Dielectric Response of Epitaxially Strained $SrTiO_3$ from First Principles. *Phys. Rev. B* **2005**, *71*, 27−29.
(6) Wu, Z.; Neaton, J. B.; Grossman, J. C. Charge Separation via Strain in Silicon Nanowires. *Nano Lett.* **2009**, *9*, 2418−2422.
(7) Nitzan, A.; Ratner, M. A. Electron Transport in Molecular Wire Junctions. *Science* **2003**, *300*, 1384−1389.
(8) Xue, Y.; Datta, S.; Ratner, M. A. First-Principles Based Matrix Green's Function Approach to Molecular Electronic Devices: General Formalism. *Chem. Phys.* **2002**, *281*, 151−170.
(9) Milliron, D. J.; Hughes, S. M.; Cui, Y.; Manna, L.; Li, J.; Wang, L.; Paul Alivisatos, A. Colloidal Nanocrystal Heterostructures with Linear and Branched Topology. *Nature* **2004**, *430*, 190−195.
(10) Shieh, F.; Saunders, A. E.; Korgel, B. A. General Shape Control of Colloidal CdS, CdSe, CdTe Quantum Rods and Quantum Rod Heterostructures. *J. Phys. Chem. B* **2005**, *109*, 8538−8542.
(11) Dorfs, D.; Salant, A.; Popov, I.; Banin, U. ZnSe Quantum Dots within CdS Nanorods: A Seededgrowth Type-II System. *Small* **2008**, *4*, 1319−1323.
(12) Sancho, M.; Sancho, J.; Sancho, J.; Rubio, J. Highly Convergent Schemes for the Calculation of Bulk and Surface Green Functions. *J. Phys. F* **1985**, *15*, 851.
(13) Niquet, Y.-M.; Delerue, C. Band Offsets, Wells, and Barriers at Nanoscale Semiconductor Heterojunctions. *Phys. Rev. B* **2011**, *84*, 1−9.
(14) Newns, D. Self-Consistent Model of Hydrogen Chemisorption. *Phys. Rev.* **1969**, *178*, 1123.
(15) Muscat, J. P.; Newns, D. M. Chemisorption on Metals. *Prog. Surf. Sci.* **1978**, *9*, 1−43.
(16) Reuter, M. G. Closed-Form Green Functions, Surface Effects, and the Importance of Dimensionality in Tight-Binding Metals. *J. Chem. Phys.* **2010**, *133*, 034703.
(17) Sadowski, T.; Ramprasad, R. Core/Shell CdSe/CdTe Heterostructure Nanowires Under Axial Strain. *J. Phys. Chem. C* **2010**, *114*, 1773−1781.
(18) Anderson, P. W. Localized Magnetic States in Metals. *Phys. Rev.* **1961**, *124*, 41−53.
(19) Fano, U. Effects of Configuration Interaction on Intensities and Phase Shifts. *Phys. Rev.* **1961**, *124*, 1866.
(20) Doyen, G.; Koetter, E.; Vigneron, J. P.; Scheffler, M. Theory of Scanning Tunneling Microscopy. *Appl. Phys. A* **1990**, *51*, 281−288.
(21) Mujica, V.; Kemp, M.; Ratner, M. A. Electron Conduction in Molecular Wires. I. A Scattering Formalism. *J. Am. Chem. Soc.* **1994**, *101*, 6849.
(22) Taylor, J. R. *Scattering Theory: The Quantum Theory of Nonrelativistic Collisions*; Dover Publications: Mineola, New York, 2006.
(23) Sakurai, J. J.; Tuan, S. F. *Modern Quantum Mechanics*; Addison-Wesley: New York, NY, 1994.
(24) Hewa-Kasakarage, N. N.; Kirsanova, M.; Nemchinov, A.; Schmall, N.; El-Khoury, P. Z.; Tarnovsky, A. N.; Zamkov, M. Radiative Recombination of Spatially Extended Excitons in (ZnSe/CdS)/CdS Heterostructured Nanorods. *J. Am. Chem. Soc.* **2009**, *131*, 1328−1334.
(25) Hewa-Kasakarage, N. N.; El-Khoury, P. Z.; Tarnovsky, A. N.; Kirsanova, M.; Nemitz, I.; Nemchinov, A.; Zamkov, M. Ultrafast Carrier Dynamics in Type II ZnSe/CdS/ZnSe Nanobarbells. *Nano* **2010**, *4*, 1837−1844.
(26) Vo, T.; Williamson, A. J.; Galli, G. First Principles Simulations of the Structural and Electronic Properties of Silicon Nanowires. *Phys. Rev. B* **2006**, *74*, 045116.
(27) Brasher, J. D.; Dy, K. S. Exact Tight-Binding Solution for Interface States and Resonances. *Phys. Rev. B* **1980**, *22*, 4868.
(28) Dy, K.; Brasher, J. D. Surface States and the Analytic Properties of Bloch Waves in the Tightbinding Approximation. *J. Phys. C* **1982**, *15*, 633.
(29) Harrison, W. A.; Tersoff, J. Tight-Binding Theory of Heterojunction Band Lineups and Interface Dipoles. *J. Vac. Sci. Technol., B* **1986**, *4*, 1068.